Laplace current deep level transient spectroscopy measurements of defect states in methylammonium lead bromide single crystals

John W. Rosenberg,[1] Matshisa J. Legodi,[2] Yevgeny Rakita,[1] David Cahen,[1,a)] and Mmantsae Diale[2,a)]
[1]*Department of Materials and Interfaces, Weizmann Institute of Science, Rehovot 76100, Israel*
[2]*Department of Physics, University of Pretoria, Private Bag X20, Hatfield 0028, South Africa*

(Received 13 July 2017; accepted 21 September 2017; published online 11 October 2017)

We present a measurement of the energies and capture cross-sections of defect states in methylammonium lead bromide ($MAPbBr_3$) single crystals. Using Laplace current deep level transient spectroscopy (I-DLTS), two prominent defects were observed with energies 0.17 eV and 0.20 eV from the band edges, and further I-DLTS measurements confirmed that these two defects are bulk defects. These results show qualitative agreement with theoretical predictions, whereby all of the observed defects behave as traps rather than as generation-recombination centers. These results provide one explanation for the high efficiencies and open-circuit voltages obtained from devices made with lead halide perovskites. *Published by AIP Publishing*. https://doi.org/10.1063/1.4995970

INTRODUCTION

In recent years, lead halide perovskites (HaPs) have attracted intense interest as the first low-cost, solution-processed absorbers which can be used in solar cells with cell efficiencies comparable with commercial thin film polycrystalline cells.[1] The higher bandgap HaPs are attractive as potential cheap add-ons to low bandgap c-Si-based cells for use in tandem cells. Also, the prospect of solar fuel production has spurred interest in those perovskites. The band gap of methylammonium lead bromide ($MAPbBr_3$), at 2.3 eV, can in principle provide a sufficiently large voltage to split water. Cells based on this material have been reported with an open-circuit voltage as high as 1.6 V.[2]

In general, if one wishes to improve solar cell performance, whether that means pushing the conversion efficiency closer to the Schockley-Queisser limit or the more limited goal of pushing the open-circuit voltage closer to the maximum value that is possible, given the band gap of the absorber, one must minimize the presence of defects in that absorber. However, in spite of the rapid improvements in efficiencies and open-circuit voltages of HaP solar cells, our fundamental understanding of the defect states in lead HaPs is cursory at best. Yin *et al*. calculated the formation energies of all possible simple point defects in methylammonium lead iodide ($MAPbI_3$) and found that the formation energies of deeper defects are so high that their formation under the conditions of synthesis of the materials is unlikely, leading them to conjecture that lead halide perovskites have mainly shallow defects.[3] However, attempts to verify this prediction by arriving at experimental estimates of the trap densities and energies have given varying results. Hutter *et al*., fitting a kinetic model to time-resolved (i.e., pulsed) photoluminescence measurements, deduced a density of $6 \times 10^{16}\,cm^{-3}$ for $MAPbI_3$ thin films and $\sim 10^{15}\,cm^{-3}$ for meso-structured $MAPbI_3$ on Al_2O_3.[4] Baumann *et al*. derived a density of $10^{15}\,cm^{-3}$ for a defect with an energy of around 500 meV from measurements of thermally stimulated current on $MAPbI_3$.[5] Duan *et al*., using thermal admittance spectroscopy, deduced the existence of two defects in a $MAPbI_3$ film at 0.167 eV and 0.35 eV above the valence band, with the defect at 0.167 eV, the density of which they calculated to be around $10^{16}\,cm^{-3}$, being attributed to iodine interstitials based on theoretical calculations.[6]

In light of the varying estimates in the literature for the energies and densities of defect states in methylammonium lead halide perovskites, we chose to use an established method to measure the defect energies and densities. Deep-level transient spectroscopy (DLTS) has been used with great success to measure the energies of defects in well-studied semiconductors such as Si and GaAs, with much of the early work on silicon being done by Sah in the 1970s.[7] The method is straightforward in the sense that one measures the emission time constant of the defects directly by analyzing the transients in current (or capacitance) at different temperatures. However, conventional, so-called "boxcar DLTS" suffers from the same precision limitation as thermal admittance spectroscopy: a defect with a well-defined energy will give a broad peak. To overcome this problem one can use Laplace DLTS, which can, in practice, surpass the resolution of conventional DLTS by about an order of magnitude, and can detect closely spaced peaks that other techniques, such as thermal admittance and thermally stimulated current, are unable to resolve. In principle, Laplace DLTS is limited only by the noise level of the measurement and the accuracy to which one can control the temperature of the sample. Since, based on the results from theoretical calculations, we can expect several defect levels closely spaced in energy near the band edges (some such levels may even be part of a family of levels related to a single defect), Laplace DLTS is an appropriate tool for measuring the energy levels of defects in methylammonium lead halide perovskites.

In this work, we have chosen to measure the energies, capture cross-sections, and densities of defect states in single crystals of the high bandgap (2.3 eV) perovskite $MAPbBr_3$

a)Authors to whom correspondence should be addressed: david.cahen@weizmann.ac.il and mmantsae.diale@up.ac.za

using current DLTS. We prepared Schottky diodes on perovskite single crystals, pulsed the diodes from reverse to forward bias, and measured the current transients observed after the pulse. From the transient, we can determine the emission rates of the defects by performing an inverse Laplace transform on the transient, and by watching how the emission rate of each defect changes with temperature, we can determine the energy and capture cross-section of the defect. We can also estimate the defect density from the magnitude of the transient itself. Based on these measurements, we have verified the conjecture that the dominant defects in lead HaPs are shallow defects.

EXPERIMENTAL METHODS

Crystals of $MAPbBr_3$ were prepared according to the procedure of Rakita *et al.*[8] A 0.5 M solution containing a 1:1 molar ratio of MABr and $PbBr_2$ in *N*,*N*-dimethylformamide (DMF) was prepared in a vial and placed in a closed container which also contained ethyl acetate, an antisolvent for $MAPbBr_3$. As the ethyl acetate vapor slowly dissolves in the DMF solution, the solubility of the perovskite decreases, resulting in the formation of cubic $MAPbBr_3$ crystals approximately within one day. Similar $MAPbBr_3$ single-crystal growth procedures and the synthesis of MABr have been described previously.[9,10]

Previous thermoelectricity measurements conducted in our lab have shown such crystals to be p-type.[11] To prepare Schottky diodes on these crystals, carbon was chosen as an ohmic contact, and gold was found to give a junction with rectification in the direction expected for a depletion layer on a p-type semiconductor. Since the ionization energy of $MAPbBr_3$ as reported in the literature is greater than the work function of gold,[12] the formation of a Schottky barrier at the Au-$MAPbBr_3$ interface is predicted by the Mott-Schottky rule. For each crystal, a 75 nm thick gold contact was deposited by e-beam evaporation and the carbon contact ($\sim$50 μm) was painted onto the crystal from carbon paste dissolved in isopropanol, a perovskite antisolvent.

The sample is kept under rough vacuum (10^{-2} mbar) in dark conditions during the measurement, and the sample is cooled by a cryostat (APD E202) using liquid helium. The temperature is monitored and controlled by a Lakeshore 333 temperature controller to a stability of 20 mK. The voltage applied across the sample is controlled by a pulse generator (Agilent 33220A), whose output is connected to the blocking contact. The current transient is measured from the ohmic contact, which is grounded through the current amplifier, and the current is changed into a voltage signal by the current amplifier (Keithley 428), which can deliver a signal to a data collection system for averaging, such as an oscilloscope. The signal is then digitized and sent to a computer for analysis. The software for triggering the pulse generator as well as averaging and analyzing the transients is contained on a Laplace card (a hardware circuit card which is inserted into the computer), which applies an inverse Laplace transform to the averaged current transient before displaying the result on the computer. A diagram of this setup is shown in Fig. 1. Further details regarding the setup may be found in Refs. 13, 14, and 15.

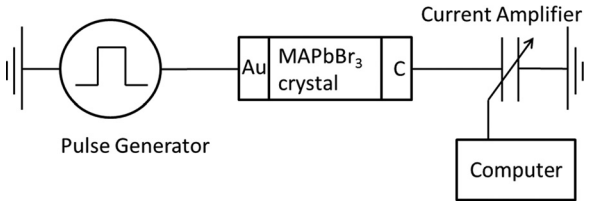

FIG. 1. A schematic of the measurement setup. A pulse generator applies a pulse from reverse bias to zero bias or to small forward bias, and a current amplifier converts the current transient flowing through the diode after the end of the pulse to a voltage signal, which is then stored, averaged for several trials (pulses), and analyzed appropriately with a computer (applying correlators with various rate windows for conventional DLTS, or performing a deconvolution routine on the entire decay curve for Laplace DLTS).

The main idea behind DLTS is to use the variation in defect emission rates with temperature to determine the difference in energy between the defect states and one of the band edges as well as to determine the capture cross-section of the defects. To see how the transient is measured, consider a point in our diode lying at the edge of the quasi-neutral region at zero bias. The traps at this point would be occupied by electrons after a long time in reverse bias [Fig. 2(c)], but when we pulse to reverse bias, this point will no longer be in the depletion region, so emission will no longer be the dominant process; rather, in a p-type material, hole capture will dominate all other processes, and in the steady state, almost all the traps will be occupied by holes [Fig. 2(a)]. Now suppose the diode is suddenly placed in reverse bias, so that the space charge region expands to include this point. During this phase, hole emission is the dominant process because emitted holes are swept out of the space charge region very quickly before they can be recaptured, resulting in a current. A long time after the pulse ends, the number of traps occupied by electrons increases, so electron emission begins to compete with hole emission, and the relative rates of the two processes dictate steady-state occupancy [Fig. 2(c)]. If a given trap lies well below the Fermi level at the given reverse bias, it is likely to be occupied by an electron. Thus, when the sample is pulsed again from reverse bias to zero bias or forward bias [change from Figs. 2(c) to 2(a)], holes will flow in and be captured by the traps which are now occupied by electrons, returning us to our original state. A diagram showing the changes in the defect state occupancy over the course of the measurement for a p-type material is shown in Fig. 2.

Thus, by keeping our diode under reverse bias [Fig. 2(c)] and pulsing to zero bias or a small forward bias for just long enough to fill the traps with holes [Fig. 2(a)], and then measuring the current after the pulse ends [Fig. 2(b)], we can measure a current transient which is due only to emission, and from the time constants of the decay of this transient we can extract the emission rates of the defects.

It is important to realize that although we expect majority carrier emission from defects to be the dominant process, when we measure the transient under reverse bias, minority carrier emission would give a current transient of the same sign, since minority carriers, having the opposite charge from the majority carriers, would be swept to the opposite direction. Therefore, we cannot empirically distinguish

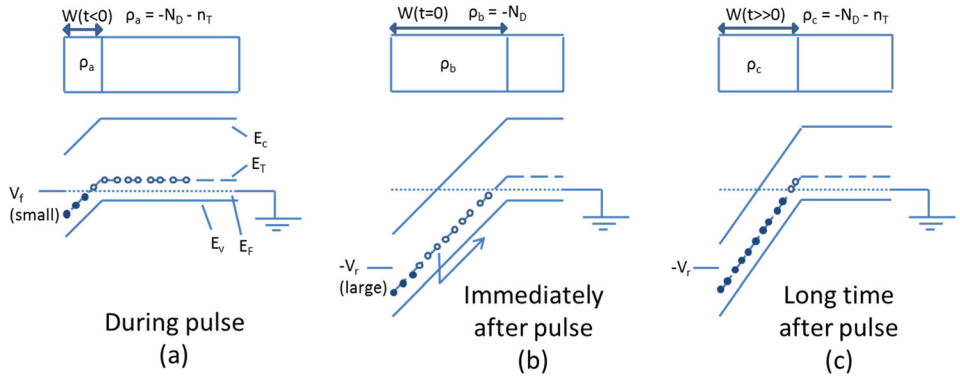

FIG. 2. A diagram of the change in the space charge region width (not to scale) in a p-type semiconductor during and after the pulse, which gives rise to the filling and emptying of the traps responsible for the transient. We start with the junction under reverse bias for a long time (c) with traps below the Fermi level occupied by electrons, then we pulse to 0 bias (a) (one can also pulse to a small forward bias), causing a dramatic contraction of the SCR [as is seen by comparing to the situation in (c)]. As a result, holes rush in to be captured by the traps which are now above the Fermi level. When the pulse ends, we return to reverse bias and the SCR greatly expands (b); the hole-occupied traps in the SCR are now below the Fermi level, so that emission of holes is the dominant process. As the holes are emitted, they leave behind electrons, which increases the density of negative charge in the SCR above the density created by the dopants, so that the band bending gradually increases and the SCR gradually contracts, returning to (c). The gradual change from (b) to (c) is where we observe the transients. In contrast to the behavior of the defects, the dopants, due to their shallow energies, are always below the Fermi level, so their occupancy is not affected by such a pulse.

between majority and minority carrier traps with current DLTS, and, thus, we do not know if the energies that we measure for each defect are to be taken relative to the valence band or to the conduction band.

The gradual change in the occupancy of the traps after the filling pulse (to zero or small forward bias) ends and the diode is returned to reverse bias also causes a change in the width of the space charge region. The space charge region in a p-type material carries a density of negative charge due to the acceptor dopants so that, as more and more traps become occupied by electrons rather than holes, the charge density in the space charge region increases, and its width decreases. Assuming a uniform charge density within the SCR, the standard relation between the charge density ρ and the space charge region (SCR) width W (for a three-dimensional SCR) is

$$W = \sqrt{\frac{2\varepsilon(V_{bi} - V)}{\rho}}, \tag{1}$$

where ε is the dielectric constant, V_{bi} is the built-in voltage, and V is the bias applied to the diode. This causes a reduction in the emission current and also induces a displacement current as charges move toward the interface of the diode to compensate for the increased charge density in the space charge region. It is simple to show that the emission current is the dominant effect, and the displacement current merely reduces the overall current by a factor of two.[16] In any case, it should be clear that as long as the overall density of traps n_T is much smaller than the doping density N_D, one can neglect the effect of the change in the width of the space charge region occurring after the return to reverse bias as a result of emission from defects (since $\rho \approx -N_D$ in any case).

Therefore, the current transient due to emission from a given trap has the form of an exponential decay

$$I = I_0 e^{-e_p t}, \tag{2}$$

where e_p is the emission rate of holes from the trap and I_0 is proportional to the trap density. We also note that because the current transient is essentially the derivative of the trap occupancy [since $\frac{dW}{dt}$ is small, we have $\frac{d}{dt}(AW(N_D + n_T)) \approx AW\frac{dn_T}{dt}$ for a junction of area A], current transients are typically fast and the magnitude of the transient will depend on the emission rate (since, during the transient, $\frac{dn_T}{dt} \approx -e_p p$, where p is the hole density) and through it, on the temperature T [see Eq. (3)]. Once we extract e_p from the transient for several temperatures, we can derive the energy and capture cross-section of a defect from the variation in emission rate with temperature—an Arrhenius plot. The emission rate from a defect is given by

$$e_{p/n} = \frac{e^{\frac{|E_T - E_{V/C}|}{k_B T}}}{T^2 \gamma_{p/n} \sigma_{p/n}}; \quad \gamma_{p/n} = 3.25 \cdot 10^{25} \left(\frac{m_{p/n}}{m_e}\right) \mathrm{cm}^{-2}\mathrm{s}^{-1}\mathrm{K}^{-2}, \tag{3}$$

where E_T is the energy of the defect state, $E_{V/C}$ is the energy of the valence or conduction band, T is the temperature, k_B is the Boltzmann constant, $\sigma_{p/n}$ is the capture cross-section of the defect state acting as a hole/electron trap, m_e is the electron rest mass in vacuum, and $m_{p/n}$ is the hole/electron effective mass, where, for $MAPbBr_3$, we use the literature value of $0.26m_e$.[17] Therefore, fitting the observed emission rates to this equation by making an Arrhenius plot of the dependence of the emission rate e_p on temperature will give the energy ($|E_T - E_{V/C}|$) and capture cross-section ($\sigma_{p/n}$) of the trap.

The practical basis of DLTS is finding a way to obtain emission rates for all the traps present in a sample when the total transient is a sum of all the exponential decays corresponding to each trap. One of the first methods developed for this purpose is to apply some functional to a transient, called a correlator, which reaches a peak when the emission rate of one of the defects responsible for the transient matches the chosen rate window of the correlator. The simplest such correlator, called the boxcar correlator, is just the difference between the transient at two times. Clearly, if the emission rate is too fast, the output will be small as the currents at

those times will both be small, and if the emission rate is too slow, the output will be small as the currents at those times will both be close to the initial current, but for some optimal, intermediate emission rate, the output will be maximized. In practice, the correlator output for a given rate window is plotted for many different temperatures, and since the emission rate of a defect increases with temperature [see Eq. (3)], there must be an optimal temperature where the emission rate matches the rate window of the correlator. Thus, the correlator output is maximized at that temperature, and we conclude that the emission rate at this temperature is given by the rate window chosen. The spectrum obtained by plotting this "boxcar" correlator output versus temperature for a given rate window is called a boxcar DLTS spectrum. Repeating this procedure for multiple rate windows should allow to produce a plot of $\ln(T^2/e)$ versus 1/T and derive the energies and capture cross-sections of the defects.

For our Au-$MAPbBr_3$-C diodes, as a preliminary measurement, conventional current DLTS measurements were conducted with a boxcar correlator for various rate windows from $5\,s^{-1}$ to $2000\,s^{-1}$. The temperature was varied from 203 K to 315 K in steps of 0.43 K ($MAPbBr_3$ remains in the tetragonal phase throughout this temperature range[18]), and the sample was held at −2 V reverse bias and pulsed to 0 V forward bias for 1 ms at each temperature.

The major disadvantage of conventional DLTS techniques such as the one described above is that even if the measurement is conducted perfectly, with no noise in the transient and perfect control over the temperature, the peaks in the spectrum will still have a finite width. Therefore, if there are multiple defects in the material with similar emission rates, their peaks may overlap and appear as a single peak in a conventional DLTS spectrum.

To resolve the peaks due to these different defects, we need a transformation which should give an arbitrarily sharp peak for an arbitrarily accurate measurement of an exponential decay due to a defect, and the inverse Laplace transform, which, given a transient $f(t)$, extracts a spectrum $F(s)$ such that $f(t) = \int_0^\infty F(s)e^{-st}ds$, has exactly this property. There are many algorithms available to obtain the inverse Laplace transform of a transient corrupted with noise; in this work, we use the CONTIN regularized deconvolution routine, which is in the public domain.

Once we know the temperature range of interest from conventional DLTS, we can return to a temperature in that range, average, save the entire observed transient, and then apply an inverse Laplace transform to obtain a spectrum which directly gives peaks at the emission rates associated with defects at that temperature. Such a spectrum is called a Laplace DLTS spectrum. Once we obtain a Laplace DLTS spectrum for several temperatures within the range of interest, we can then produce a separate Arrhenius plot for each defect level and derive their energies and capture cross-sections. In practice, since the deconvolution method itself no longer limits our resolution, and we are limited only by the noise level and the temperature drift, Laplace DLTS allows us to separate closely spaced peaks with a resolution an order of magnitude better than what can be obtained with conventional DLTS. Typically, conventional DLTS can resolve two peaks with a ratio of emission rates ≥15, whereas Laplace DLTS can resolve two peaks with a ratio of emission rates as low as 2.[14] This superior resolution makes Laplace DLTS a fitting tool for studying defects in lead halide perovskites, since several theoretical computations predict that these materials may have densely spaced defect levels close to the band edges.

For our Au-$MAPbBr_3$-C diodes, Laplace spectra were derived from averaged current transients measured at temperatures from 300 K to 275 K. The sample was held at −4 V reverse bias and pulsed to +1 V forward bias for 1 ms to ensure that all defect states within the band gap would capture and emit carriers. The transient was measured for 4 ms after the end of the pulse and 4000 trials were averaged before performing each deconvolution. During the measurement, we always tested for consistency with results from a different deconvolution engine, and we used as a rule of thumb that a S/N ratio of 10^4 is needed to distinguish between two peaks of the same height with emission rates differing by a factor of 2.[16] In our measurements, our S/N ratio was typically 10^3, so we made sure to record transients for a length of time no shorter than (7/e) for an emission rate e. (The noise in the transient is likely due to multiple factors, including temperature instability, noise pickup during analog-to-digital conversion, and sample noise.)

RESULTS AND DISCUSSION

Results of the preliminary conventional DLTS measurements are shown in Fig. 3.

The spectra from the four fastest rate windows—$200\,s^{-1}$, $500\,s^{-1}$, $1000\,s^{-1}$, and $2000\,s^{-1}$—show very broad peaks, with the largest correlator outputs observed in the 275–300 K temperature range. The positions of these peaks can be fitted to an Arrhenius plot and assigned to a single defect with an energy of 0.23 eV and a capture cross-section

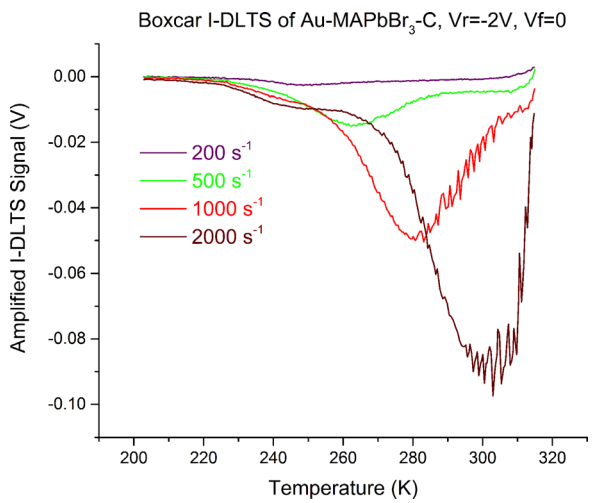

FIG. 3. Conventional DLTS spectra for the four fastest rate windows measured as the temperature is varied from 203 K to 315 K. The sample was held at reverse bias $V_r = -2$ V and pulsed to forward bias $V_f = 0$ V for 1 ms at each temperature. Large correlator outputs were observed between 275 K and 300 K, indicating the presence of one or more defects with similar emission rates to these rate windows in this temperature range. We used an amplification of 10^7 V/A.

of 2×10^{-19} cm^2, but given the large width of the peaks, it is likely that multiple defects contribute to each peak, and that conventional current DLTS measurements lack the resolution necessary to distinguish the closely spaced energies of these defects. Thus, we conducted Laplace DLTS measurements in the 275–300 K temperature range to check if there are multiple peaks (i.e., multiple defect levels).

A typical set of Laplace spectra is shown in Fig. 4.

The CONTIN routine generated these spectra via a discrete deconvolution using 200 points sampled from the transient, which were fitted to a model with 200 emission rates. The magnitude of the full amplified transient may be obtained by summing the spectral density at each of these 200 emission rates.

Each spectrum shows two large peaks in the 10^2–10^4 s^{-1} range and a smaller peak above 10^4 s^{-1}; the 280 K and 275 K spectra show, in addition, an even smaller peak around 4×10^4 s^{-1}. The two large peaks were also observed in spectra taken from other samples, whereas the smaller peaks were observed only in this sample. For defects, the emission rate is expected to increase with temperature, and this is indeed what we observe for all of the peaks in this set of spectra, with the exception of the small peak above 10^4 s^{-1} in the 295 K spectrum, which occurs at a faster rate than that of the 300 K spectrum. This may be due to the fact that the position of smaller peaks is given less accurately by inverse Laplace deconvolution routines than that of larger peaks because once one has already accounted for the larger peaks, the effective S/N ratio for the smaller peak's contribution to the transient is larger, which, during deconvolution, introduces a greater spreading of the position of this peak.

Once we have recorded the emission rate of each peak in the Laplace spectrum at each temperature, we plot ln(T^2/e) versus 1/T, and we can then derive the energy $|E_T\text{-}E_{V/C}|$ and the capture cross-section $\sigma_{p/n}$ for the defect from the slope and intercept of the Arrhenius plot, respectively [see Eq. (3)]. Arrhenius plots for the two large, reproducible peaks seen in the set of spectra above are shown in Figs. 5 and 6.

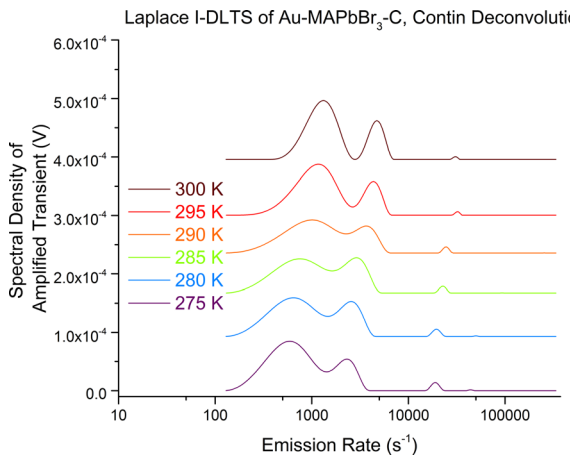

FIG. 4. Laplace DLTS spectra for various temperatures between 275 K and 300 K, obtained using the CONTIN deconvolution routine. The sample was held at −4 V reverse bias and pulsed to +1 V forward bias for 1 ms, and the resulting transient was measured 4000 times at each temperature with an amplification of 10^7 V/A and averaged before performing each deconvolution. Each spectrum shows two large peaks in the 10^2–10^4 s^{-1} range and a smaller peak above 10^4 s^{-1}, all of whose emission rates increase with increasing temperature, consistent with the presence of three defects, though only the two large peaks were observed in other similarly prepared samples.

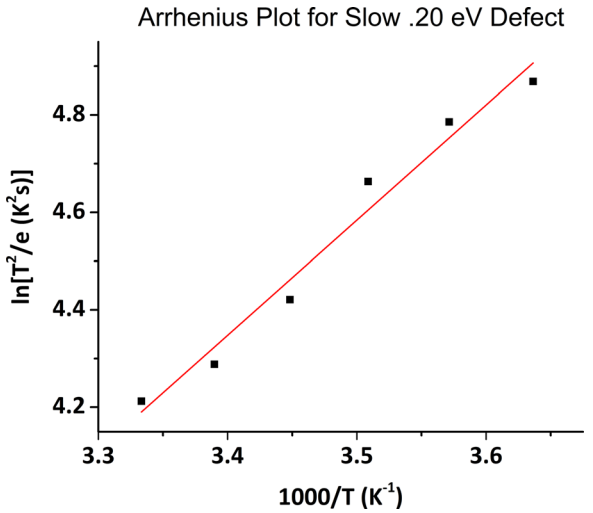

FIG. 5. An Arrhenius plot of the slower of the two larger peaks, derived from the temperature T and the emission rate e corresponding to the peaks in spectral density in Fig. 3. The data show good agreement with the model in Eq. (3) ($R^2 = 0.975$) and are consistent with the presence of a defect with an energy 0.204 ± 0.016 eV from one of the band edges.

Results show good agreement with the model given by Eq. (3), and we can see from the Arrhenius plots that of the two large peaks observed, the large peak with the slower emission rate is due to a defect with an energy of 0.204 ± 0.016 eV and a capture cross-section of 5×10^{-20} cm^2 (ln(σ/cm^2) = −44.5 ± 0.7), and the large peak with the faster emission rate is due to a defect with an energy of 0.167 ± 0.014 eV and a capture cross-section of 4×10^{-20} cm^2 (ln(σ/cm^2) = −44.7 ± 0.6). The faster small peak also shows satisfactory agreement with the model and may indicate a defect with an energy of 0.113 ± 0.027 eV and a capture cross-section of 3×10^{-20} cm^2 (ln(σ/cm^2) = −44.8 ± 0.4). The small capture cross-sections may indicate that re-trapping

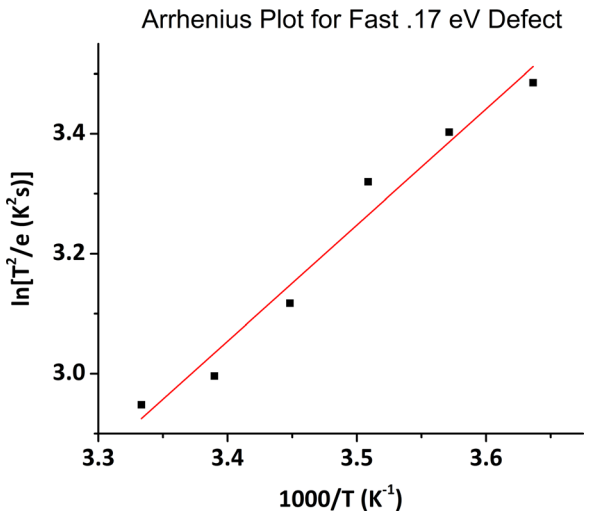

FIG. 6. An Arrhenius plot of the faster of the two larger peaks, derived from the temperature T and the emission rate e corresponding to the peaks in spectral density from Fig. 3. The data show good agreement with the model in Eq. (1) ($R^2 = 0.972$) and are consistent with the presence of a defect with an energy 0.167 ± 0.014 eV from one of the band edges.

is unlikely. These results agree with theoretical predictions that the dominant defect states in lead halide perovskites are shallow and behave as traps rather than as generation-recombination centers.[3]

Given that the properties of diodes produced from lead HaPs often change under illumination, we also attempted to measure these samples immediately after exposing them to the light and then returning them to dark conditions. We were unable to obtain stable results from these experiments, so that further work is needed to determine the preconditioning necessary to model the behavior of the defects in the lead HaP under working conditions.

Although we expect negligible activity from surface and interfacial states given the fast transients, we suspected that a forward bias of +1 V might still access them. Therefore we conducted a series of control measurements with smaller pulse heights, to rule out the contribution of surface states. The reverse bias was maintained at −4 V and the forward bias of the pulse was varied from −3.9 V to −2.6 V, thus changing the width of the emission region from 20 μm to 350 μm. (The derivation of these widths from the biases can be found in the supplementary material.) The heights of the two largest peaks in the Laplace spectrum at 280 K were measured as a function of the forward bias. The third smaller peak was not observed in these measurements, so we cannot be certain as to its origin. A plot of the peak height versus the width of the emission region (the amount by which the SCR contracts during the pulse) for each of the two large peaks in the Laplace spectrum is shown in the supplementary material in Fig. S1 (supplementary material).

If these defects occurred only at the interface with the contacts, we would expect to see no dependence of the peak height on the forward bias, and if the defects occurred only at the surface, we would see a non-linear dependence of the peak height on the calculated emission region width [calculated as $W(V_r)$-$W(V_f)$ from Eq. (1), where V_r and V_f are the voltages applied to the diode under forward and reverse bias, respectively]. As the peak height shows a linear dependence on the width of the emission region for both of these peaks, this indicates that the defects responsible for the two large peaks in the Laplace spectrum are bulk defects and are not due to the deposition of the contacts. We can also conclude from the linear dependence that these bulk defects have a uniform distribution throughout the sample.

An estimate for the densities of the defects may be obtained using the equation for the magnitudes of the current transients

$$I_k = \frac{qAWe_k}{2}\frac{n_k}{\sqrt{1-\frac{\sum_k n_k}{N_D}}} \approx \frac{qAWe_k n_k}{2}, \tag{4}$$

where I_k is the magnitude of the current transient resulting from the kth defect, e_k is the emission rate of the kth defect, n_k is the density of the kth defect, N_D is the doping density, W is the width of the depletion region immediately after the return to reverse bias, A is the area of the Schottky contact, and q is the electron charge.[16] We use the reported carrier density of the p-doped $MAPbBr_3$ crystal, $N_D = 10^{10}\,cm^{-3}$.[10] With that value we find that the density of the 0.20 eV defect is on the order of $10^9\,cm^{-3}$, the density of the 0.17 eV defect is on the order of $10^8\,cm^{-3}$, and the density of the 0.11 eV defect, that was found in one of the samples, is on the order of $10^6\,cm^{-3}$. (Note that $N_D \gg \sum_k n_k$ justifies our use of the simple inverse Laplace transform to determine the defect emission rates.) Furthermore, an overall trap density on the order of $10^9\,cm^{-3}$ agrees with previous space charge-limited current (SCLC) measurements of defect densities in a single crystal of $MAPbBr_3$.[10]

CONCLUSION

Using Laplace I-DLTS, we measured the energies and capture cross-sections of defect states in single crystals of the $MAPbBr_3$ perovskite. The Laplace spectra indicate the presence of two fairly shallow defects: one defect with an energy of 0.167 ± 0.014 eV, a capture cross-section of 4×10^{-20} cm^2 ($\ln(\sigma/\text{cm}^2) = -44.7 \pm 0.6$), and an approximate density of $10^8\,cm^{-3}$ contributing a fast decay, and another defect with an energy of 0.204 ± 0.016 eV, a capture cross-section of 5×10^{-20} cm^2 ($\ln(\sigma/\text{cm}^2) = -44.5 \pm 0.7$), and an approximate density of $10^9\,cm^{-3}$ contributing a slow decay. These results are consistent with theoretical predictions which implied that all of the defects present at a significant density in methylammonium lead HaPs should be shallow defects, which are more likely to behave as traps than as G-R centers. In addition, the linear dependence of the spectral density of these two defects on the calculated width of the emission region shows that they are bulk defects and are not due to the deposition of the contacts.

Although we have measured the densities, energies, and capture cross-sections of the defect states, we have made no claim regarding the chemical nature of the defects. Future DLTS measurements on lead HaPs should attempt to determine the changes in defect states caused by various treatments, such as exposure to halogens, or illumination with different frequencies of light.

Overall, we have shown that Laplace DLTS is a useful tool for analyzing the nature of defect states in lead HaPs due to its superior resolution. In addition, our measurements support one possible explanation for the high efficiencies and open-circuit voltages observed in perovskite solar cells: namely, that the defects present in lead HaPs are shallow defects and therefore do not cause as much recombination as deeper defects would. Thus, in spite of the fact that the density of defects is not exceptionally small relative to the carrier density, their shallow position within the band gap allows one to produce solar cells with high efficiencies and open-circuit voltages from these materials.

SUPPLEMENTARY MATERIAL

See supplementary material for a plot of the peak height versus the width of the emission region for each of the two large peaks observed in the Laplace spectrum, along with a derivation of the width of the emission region using the literature values for the valence band edge energy E_v for $MAPbBr_3$[12] and for the doping density N_D and permittivity ε.[8]

ACKNOWLEDGMENTS

The DLTS setup, including hardware and software, was provided to the Diale lab by A. R. Peaker (Center for the electronic Materials Devices and Nanostructures, University of Manchester), and L. Dobaczewksi (Institute of Physics, Polish Academy of Sciences).

We thank Professor François D. Auret for many fruitful discussions regarding DLTS, along with much helpful advice regarding the experimental procedures and Professor Gary Hodes for helpful discussions regarding the interpretation of these results. We thank Hadar Kaslasi for providing several crystals that we used to test our diode configuration. At the WIS this work was supported in part by the Israel Ministry of Science's Tashtiot program. At U Pretoria this work was supported in part by the NRF Nanotechnology Flagship Program (Project No. 88021). D.C. holds the Sylvia and Rowland Schaefer Chair in Energy Research.

[1]A. M. Ganose, C. N. Savory, and D. O. Scanlon, "Beyond methylammonium lead iodide: Prospects for the emergent field of ns^2 containing solar absorbers," Chem. Commun. **53**(1), 20–44 (2017).
[2]C. G. Wu, C. H. Chiang, and S. H. Chang, "A perovskite cell with a record-high-V-oc of 1.61 V based on solvent annealed $CH_3NH_3PbBr_3$/ICBA active layer," Nanoscale **8**(7), 4077–4085 (2016).
[3]W. J. Yin, T. T. Shi, and Y. F. Yan, "Unique properties of halide perovskites as possible origins of the superior solar cell performance," Adv. Mater. **26**(27), 4653 (2014).
[4]E. M. Hutter *et al.*, "Charge carriers in planar and meso-structured organic-inorganic perovskites: Mobilities, lifetimes, and concentrations of trap states," J. Phys. Chem. Lett. **6**(15), 3082–3090 (2015).
[5]A. Baumann *et al.*, "Identification of trap states in perovskite solar cells," J. Phys. Chem. Lett. **6**(12), 2350–2354 (2015).
[6]H. S. Duan *et al.*, "The identification and characterization of defect states in hybrid organic-inorganic perovskite photovoltaics," Phys. Chem. Chem. Phys. **17**(1), 112–116 (2015).
[7]C. T. Sah, "Bulk and interface imperfections in semiconductors," Solid-State Electron. **19**(12), 975–990 (1976).
[8]Y. Rakita *et al.*, "$CH_3NH_3PbBr_3$ is not pyroelectric, excluding ferroelectric-enhanced photovoltaic performance," APL Mater. **4**(5), 051101 (2016).
[9]Y. Tidhar *et al.*, "Crystallization of methyl ammonium lead halide perovskites: Implications for photovoltaic applications," J. Am. Chem. Soc. **136**(38), 13249–13256 (2014).
[10]D. Shi *et al.*, "Low trap-state density and long carrier diffusion in organolead trihalide perovskite single crystals," Science **347**(6221), 519–522 (2015).
[11]Y. Rakita *et al.*, "Tetragonal $CH_3NH_3PbI_3$ is ferroelectric," Proc. Natl. Acad. Sci. U.S.A. **114**(28), E5504–E5512 (2017).
[12]P. Schulz *et al.*, "Interface energetics in organo-metal halide perovskite-based photovoltaic cells," Energy Environ. Sci. **7**(4), 1377–1381 (2014).
[13]W. Mtangi, *Electrical Characterization of Process, Annealing, and Irradiation Induced Defects in ZnO, in University of Pretoria: Faculty of Natural and Agricultural Sciences* (University of Pretoria, Pretoria, South Africa, 2012), pp. 64–67.
[14]L. Dobaczewski, A. R. Peaker, and K. B. Nielsen, "Laplace-transform deep-level spectroscopy: The technique and its applications to the study of point defects in semiconductors," J. Appl. Phys. **96**(9), 4689–4728 (2004).
[15]L. Dobaczewski, see http://info.ifpan.edu.pl/Dodatki/WordPress/laplacedlts/ for Laplace DLTS; accessed 10 July 2017.
[16]D. K. Schroder, *Semiconductor Material and Device Characterization* (Wiley-Interscience, 1990).
[17]T. M. Brenner *et al.*, "Hybrid organic-inorganic perovskites: low-cost semiconductors with intriguing charge-transport properties," Nat. Rev. Mater. **1**, 15007 (2016).
[18]O. Knop *et al.*, "Alkylammonium lead halides.2. $CH_3NH_3PbCl_3$, $CH_3NH_3PbBr_3$, $CH_3NH_3PbI_3$ perovskites - cuboctahedral halide cages with isotropic cation reorientation," Can. J. Chem. – Rev. Can. Chim. **68**(3), 412–422 (1990).